DOI: 10.1002/ejic.200501136

Synthesis, Structure, Electrochemistry, and Metal-Atom Dynamics of Cyclopentadienyl Ferracarboranes

Rolfe H. Herber,*[a] Alexander R. Kudinov,[b] Piero Zanello,[c] Israel Nowik,[a] Dmitry S. Perekalin,[b] Vladimir I. Meshcheryakov,[b] Konstantin A. Lyssenko,[b] Maddalena Corsini,[c] and Serena Fedi[c]

Keywords: Cyclopentadienyl ferracarboranes / Electrochemistry / X-ray diffraction / Mössbauer spectroscopy

A series of metallacarboranes, incorporating the CpFe fragment, were studied by electrochemical techniques, temperature-dependent Mössbauer effect (ME) spectroscopy, and X-ray diffraction. The compounds studied include the parent dicarbollide complex $CpFeC_2B_9H_{11}$ (**1**) and its reduced form [**1**]$^-$, the charge-compensated ferradicarbollides 1-Cp-4-L-1,2,3-$FeC_2B_9H_{10}$ [L = SMe_2 (**2a**), NMe_3 (**2b**), py (**2c**)] and their methylated analogs 1-Cp-2,3-Me_2-4-SMe_2-1,2,3-$FeC_2B_9H_8$ (**2d**) and 1-Cp*-4-SMe_2-1,2,3-$FeC_2B_9H_{10}$ (**2e**), the isomeric ferratricarbollides $CpFeC_3B_8H_{11}$ (**3a–c**), and the amino-substituted derivative 1-Cp-12-*t*BuNH-1,2,4,12-$FeC_3B_8H_{10}$ (**3d**). The ferradicarbollides **2a–e** were synthesized by reactions of the charge-compensated dicarbollide anions [9-L-7,8-R_2-7,8-$C_2B_9H_8$]$^-$ (R = H, Me) with [(C_5R_5)-$Fe(MeCN)_3$]$^+$ cations. The structures of **1**, [NMe_3Ph][**1**], and **2b** were investigated by X-ray diffraction. The ME spectroscopic study elucidated the relationship between the nature of the five-membered carborane face coordinated to the metal center and the hyperfine interaction parameters of the Fe atom. Temperature-dependent recoil-free fraction studies yielded the root-mean-square-amplitude-of-vibration (rmsav) of the metal atom over a wide temperature range, which proved to be in good agreement with crystallographic $U_{i,j}$ data for **1** and **3a**,**b**. Electrochemistry shows that the isomeric ferratricarbollides **3a–c** undergo reversible oxidation to the corresponding Fe^{III} derivatives at potential values higher, on average, by about 0.4 V than those of the charge-compensated complexes **2a–c** and by about 0.8 V than that of the parent ferradicarbollide [**1**]$^-$. This result indicates the strong electron-withdrawing ability of the extra carbon atom relative to that of the replaced boron atom. As a consequence of the shift of the HOMO–LUMO frontier orbitals to the high energy levels, the Fe^{II}/Fe^{I} reduction becomes accessible.

Introduction

Similar to ferrocene, the ferracarborane anion $[CpFeC_2B_9H_{11}]^-$ ([**1**]$^-$)[1] can be easily oxidized to give the neutral compound $CpFeC_2B_9H_{11}$ (**1**) which contains Fe^{III}. However, different charges of the $[C_2B_9H_{11}]^{2-}$ and Cp^- ligands lead to significant differences in the properties of [**1**]$^-$ and $FeCp_2$. Usage of monoanionic carborane ligands of two types, [9-L-7,8-$C_2B_9H_{10}$]$^-$ and $[C_3B_8H_{11}]^-$, allows one to obtain closer analogs of ferrocene such as charge-compensated ferradicarbollides **2a–e** and ferratricarbollides **3a–d** (Scheme 1). Herein we describe the synthesis and structural, electrochemical, and Mössbauer studies of these compounds, along with a reinvestigation of key metallacarboranes **1** and [**1**]$^-$.

[a] Racah Institute of Physics, The Hebrew University, 91904 Jerusalem, Israel
E-mail: herber@vms.huji.ac.il
[b] A. N. Nesmeyanov Institute of Organoelement Compounds, Russian Academy of Sciences, 119991 Moscow, Russian Federation
E-mail: arkudinov@ineos.ac.ru
[c] Department of Chemistry, University of Siena, 53100 Siena, Italy
E-mail: zanello@unisi.it

Supporting information for this article is available on the WWW under http://www.eurjic.org or from the author.

Results and Discussion

Synthesis

The charge-compensated ferradicarbollides **2a–c** were prepared by reactions of anions [9-L-7,8-$C_2B_9H_{10}$]$^-$ with the acetonitrile complex $[CpFe(MeCN)_3]^+$ (Scheme 2).[2] The starting iron complex is stable only below –40 °C,[3] and therefore its in situ generation by irradiation of $[CpFe(C_6H_6)]^+$ in a mixture of MeCN/THF and further complexation were carried out at low temperature. The analogous reaction of [9-SMe_2-7,8-Me_2-7,8-$C_2B_9H_8$]$^-$ gave the cage-methylated derivative **2d**. The ring-methylated complex **2e** was prepared by reaction of [9-SMe_2-7,8-$C_2B_9H_{10}$]$^-$ with $[Cp^*Fe(MeCN)_3]^+$.[4]

Ferratricarbollides **3a**[5] and **3d**[6] were recently obtained by room-temperature photochemical reaction of the tricarbollide anions [7-R-7,8,9-$C_3B_9H_{10}$]$^-$ (R = H, *t*BuNH) with $[CpFe(C_6H_6)]^+$, while compounds **3b** and **3c** were prepared by stepwise thermal rearrangement of **3a**.[5]

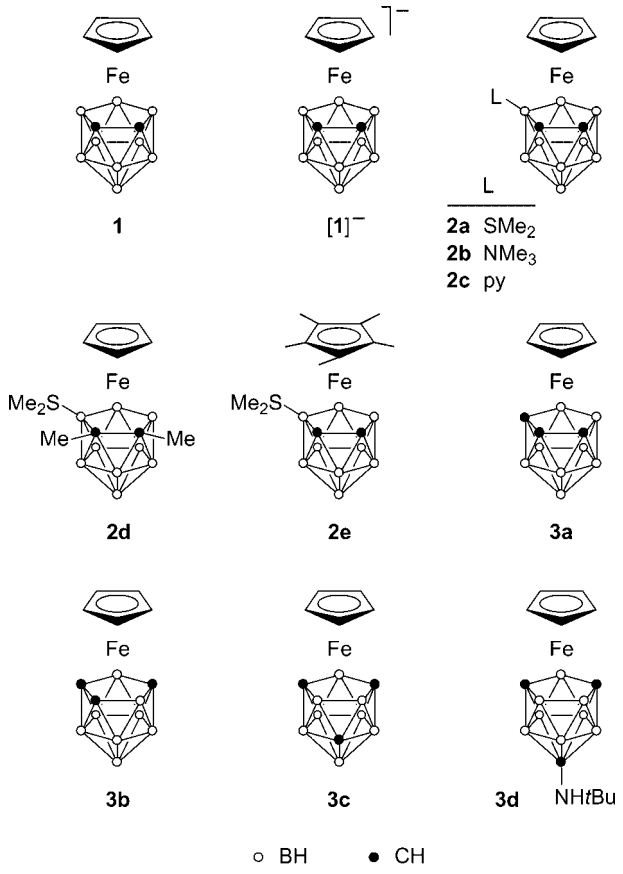

Scheme 1.

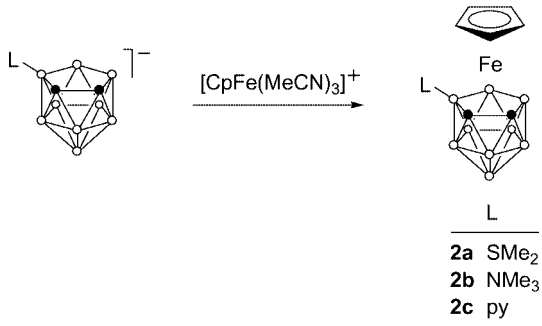

Scheme 2.

Structures

The structure of ferradicarbollide **1** was studied by X-ray diffraction in 1965, but the instrumental limitations of that time resulted in approximate data only, with significant uncertainty (ca. 0.05 Å) caused by large thermal motion.[7] Low-temperature experiments allowed us to obtain highly accurate structures of **1** and its reduced form $[\mathbf{1}]^-$ (as a $[NMe_3Ph]^+$ salt) with only minor librations of the Cp rings (Figure 1 and Figure 2).[8]

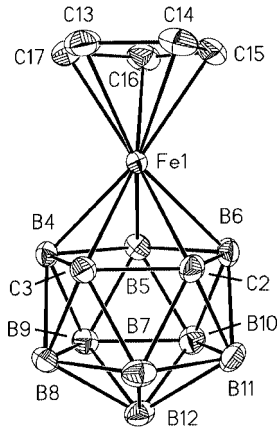

Figure 1. The molecular structure of anion $[\mathbf{1}]^-$ (thermal ellipsoids at 50% probability). Hydrogen atoms are omitted for clarity. Selected interatomic distances [Å]: Fe1–C2 2.0101(7), Fe1–C3 2.0108(7), Fe1–B4 2.0709(7), Fe1–B5 2.1090(7), Fe1–B6 2.0749(8), Fe1–C13 2.0721(7), Fe1–C14 2.0649(7), Fe1–C15 2.0514(7), Fe1–C16 2.0441(7), Fe1–C17 2.0606(7), C3–C2 1.6324(10).

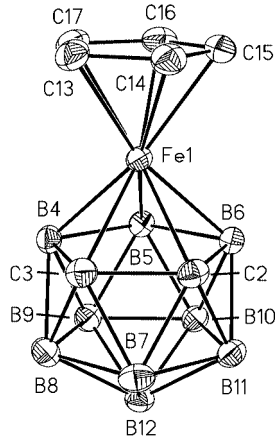

Figure 2. The molecular structure of **1** (thermal ellipsoids at 50% probability). Hydrogen atoms are omitted for clarity. Selected interatomic distances [Å]: Fe1–C16 2.0651(11), Fe1–C2 2.0716(9), Fe1–C3 2.0773(9), Fe1–C17 2.0893(11), Fe1–B6 2.0952(11), Fe1–C15 2.0961(10), Fe1–B4 2.1017(10), Fe1–B5 2.1079(11), Fe1–C13 2.1356(11), Fe1–C14 2.1399(11), C2–C3 1.6002(13).

The structure of the 18-electron anion $[\mathbf{1}]^-$ possesses a classical sandwich geometry with the Fe···C_2B_3 and Fe···C_5 distances equal to 1.437 and 1.663 Å, respectively. It is noteworthy that the latter value is very close to that in ferrocene[9] (1.660 Å), confirming a similarity of their electronic structures. The C_2B_3 and C_5 rings are nearly eclipsed (torsion angle 14°) and almost parallel (1.6°) to each other. The C_2B_3 face is notably nonplanar with the central B5 atom deviating from the B6–C2–C3–B4 plane by 0.061 Å away from the iron atom. Similar distortion was previously observed in structures of **3a**,**b**.[5]

The structure of the 17-electron neutral compound **1** is significantly different from anion $[\mathbf{1}]^-$. Both the Fe···C_2B_3 (1.487 Å) and Fe···C_5 (1.723 Å) distances in **1** are ca. 0.05 Å longer than those in $[\mathbf{1}]^-$. The latter distance is also longer than that in the similar 17-electron $[FeCp_2]^+$ cation (1.706 Å).[10] The C_5 ring is almost perfectly eclipsed with

C_2B_3 (torsion angle 4.5°) and inclined by 4.6° away from the cage carbon atoms. The C_{Carb}–C_{Carb} and average C_{Cp}–C_{Cp} distances in **1** (1.594 and 1.401 Å, respectively) are considerably shorter than those in [**1**]$^-$ (1.640 and 1.430 Å, respectively).

In order to arrive at a MO explanation for the difference between the structures of **1** and [**1**]$^-$, we carried out DFT calculations (at B3LYP/6-31G* level) of the anion [**1**]$^-$. It was found that the HOMO (Figure 3) is similar to the e_{2g}/$d_{x^2-y^2}$ orbital of ferrocene, with bonding for Fe···C_2B_3 and Fe···Cp interactions and antibonding for C_{Cp}–C_{Cp} and C_{Carb}–C_{Carb} interactions.[11] Accordingly, removal of one electron from this orbital leads to the lengthening of Fe···C_2B_3 and Fe···Cp distances and shortening of C_{Cp}–C_{Cp} and C_{Carb}–C_{Carb} distances.

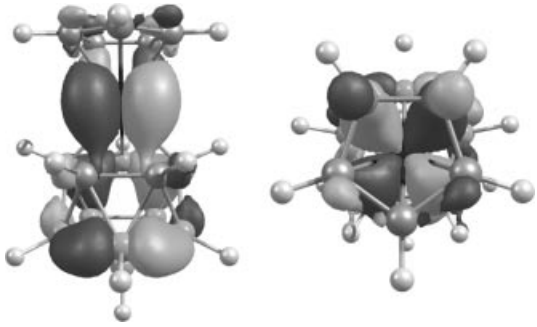

Figure 3. The plot of the HOMO of [**1**]$^-$.

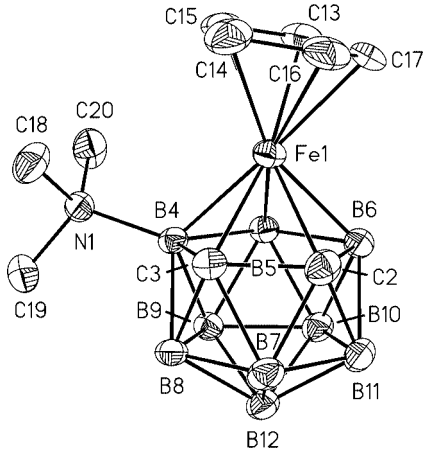

Figure 4. The molecular structure of **2b** (thermal ellipsoids at 30% probability). The second conformation of the disordered Cp ring and hydrogen atoms are omitted for clarity. Selected interatomic distances [Å]: Fe1–C2 1.995(3), Fe1–C3 2.018(3), Fe1–B4 2.108(4), Fe1–B5 2.113(3), Fe1–B6 2.072(3), Fe1–C17 2.054(9), Fe1–C16 2.079(6), Fe1–C13 2.082(7), Fe1–C14 2.091(6), Fe1–C15 2.093(5), C2–C3 1.632(5), N1–B4 1.611(4).

The structure of the charge-compensated ferradicarbollide **2b** was also confirmed by X-ray diffraction (Figure 4). In contrast to [**1**]$^-$ and **1**, the Cp ligand is disordered over two positions. The presence of the bulky NMe_3 substituent leads to the significantly bent sandwich geometry with a 9.7° angle between C_5 and C_2B_3 planes. The Fe···Cp and Fe···C_2B_3 distances (1.690 and 1.451 Å, respectively) are ca. 0.03 Å longer than those in [**1**]$^-$, probably also a result of the steric repulsion.

Mössbauer Study

Similar to other neutral, diamagnetic ferrocenoid compounds, all of the cyclopentadienyl ferracarboranes examined in the present study, namely **1**, [NMe_3Ph][**1**], **2a**,**c**, and **3a**–**d**, display a ME resonance which consists of a single, well-separated doublet spectrum characterized by its isomer shift (IS), quadrupole splitting (QS), and area under the resonance curve (A). A representative spectrum of **3c** at 92 K is shown in Figure 5. The IS and QS values at 90 K, as well as the parameters derived from the temperature-dependent data for all of the compounds are summarized in Table 1. In the following discussion, the trends in the ME hyperfine parameters are discussed in some detail.

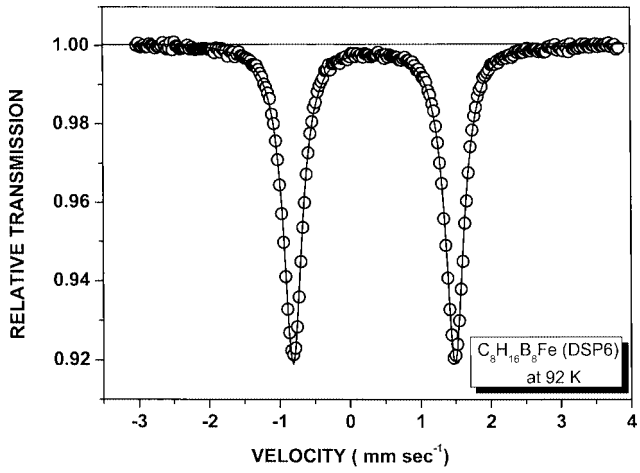

Figure 5. ^{57}Fe Mössbauer spectrum of **3c** ("DSP-6") at 92 K. The velocity scale is with reference to the centroid of a room-temperature α-Fe spectrum which was also used for spectrometer calibration.

Table 1. ^{57}Fe Mössbauer parameters for the compounds discussed in the text.

	1	[NMe_3Ph][**1**]	**2a**	**2c**	**3a**	**3b**	**3c**	**3d**	Units
IS(90)	0.337(3)	0.357(3)	0.383(5)	0.380(4)	0.430(3)	0.439(4)	0.344(4)	0.344(3)	$mm\,s^{-1}$
QS(90)	0.525(3)	2.431(3)	2.490(5)	2.480(4)	2.501(3)	2.471(5)	2.302(4)	2.360(3)	$mm\,s^{-1}$
–d(IS)/d(T)	5.3(3)	5.5(4)	5.1(5)	6.8(1)	5.1(1)	4.0(1)	4.8(4)	4.8(1)	$10^{-4}\,mm\,s^{-1}$
–d(ln A)/d(T)	7.9(1)	15.9(2)	6.3(5)	5.4(2)	4.4(3)	5.9(3)	6.7(2)	11.3(11)	$10^{-3}\,K^{-1}$
M_{eff}	78(4)	76(5)	82(3)	n.a.	100(1)	103(3)	86(3)	86(1)	Da
Θ_M	113	80	123	–	131	–	116	89	K

Isomer Shift

The IS parameters show a distinct partition into two groups: those which pertain to the ferracarboranes in which two carbon atoms of the five-membered carborane face interact with the metal atom (e.g., **3c** and **3d**), and those in which there are three carbon atoms in the pentagonal ring (e.g., **3a** and **3b**). As is evident from the electronegativity of carbon and boron and also in accordance with the results of previous DFT calculations,[5] the C atoms of the framework are more negatively charged than the B atoms. This greater electron density, which is reflected in greater shielding of the nearby iron nucleus, results in a larger IS, since it is well established that $\delta R/R$ for the 14.4 keV level of ^{57}Fe is negative.[12] The average difference in the IS parameter between the B_2C_3 and B_3C_2 compounds is almost 0.1 mm s^{-1}, a value some 30 times greater than the experimental errors in the individual measurements. An argument which further bolsters this explanation is based on the observation that other iron carboranes, in which the carborane ligand contains three carbon atoms (of which only two are located in the pentagonal ring facing the metal atom) (e.g., **3c** and **3d**), show an IS which is close to those reported for the C_2B_3 complexes noted earlier.

The temperature dependence of the IS, –d(IS)/d(T), is negative for all of the compounds examined, in consonance with similar observations reported earlier for ferrocene-related complexes. For **3a**–**c**, this temperature dependence is linear within experimental error over the accessible range of temperatures, and the corresponding values are included in the data listed in Table 1. A representative data set is shown in Figure 6. For [NMe_3Ph][**1**], **2a**, and **3d**, the data are better approximated by two linear segments, with a minor break at $T \approx 230$ K. Again, a representative data set is included in Figure 6. For **2c**, the temperature dependence of the IS parameter shows continuous curvature, and no effort was made to separate two regions of the T range in this case. As indicated in the literature,[13] the value of the –d(IS)/d(T) parameter (in the high-temperature limit) can be used to extract an effective vibrating mass, M_{eff}, for the ME active atom, and the corresponding values for the cyclopentadienyl iron carboranes of the present study fall into the range of 82 ± 4 Da for the five B_3C_2 compounds and 102 ± 4 Da for the two B_2C_3 compounds. The difference between these values and the "bare atom" iron mass of 57 Da reflects the covalence of the metal–ligand interaction, and is consistent with a larger electron density of the ring in the latter than in the former compounds, as mentioned earlier.

Quadrupole Splitting

The QS parameters at 90 K are included in the data summarized in Table 1. With the exception of the value for **1**, the data again fall into two groups: those with the B_2C_3 ring structure and those with the B_3C_2 configuration. At 90 K, the former have a QS ≈ 2.49 mm s^{-1}, while the latter have a QS ≈ 2.36 mm s^{-1}. However, it should be noted that the QS parameters are temperature-dependent, and (with some minor variations) show the normal decrease with increasing temperature because of the effects on the field gradient arising from thermal expansion. A typical data set showing this temperature dependence is shown in Figure 7. An exception to the earlier generalization is the data for the QS of **1**, which is smaller by about a factor of 4.6 than the values for the remainder of the carboranes reported here. This difference is readily understood in terms of the formal +3 oxidation state of the iron atom in **1** compared with the divalent state in the remainder. As has been previously noted[14] for ferrocene-related compounds, the removal of one electron from the metal atom on oxidation incurs an almost complete collapse of the QS, as has been discussed in detail in a classic paper by Collins[14] and elsewhere.[15] Typically, the change in the QS parameter on oxidation of the neutral parent compound is from 2.57 to 0.15 mm s^{-1} for octamethylferrocene and the corresponding cation as BF_4^- and PF_6^- salts,[16] from 2.42 to 0.21 mm s^{-1} for a bis-(isodicyclopentadienyl)iron complex and the cation as a PF_6^- salt,[17] and from 2.41 to 0.15 mm s^{-1} for ethynyloctamethylferrocene and the cation as a PF_6^- salt.[18] In the case of **1**, the QS parameter at 90 K is 0.525 ± 0.003 mm s^{-1}, presumably due to the presence of both B and C atoms in the

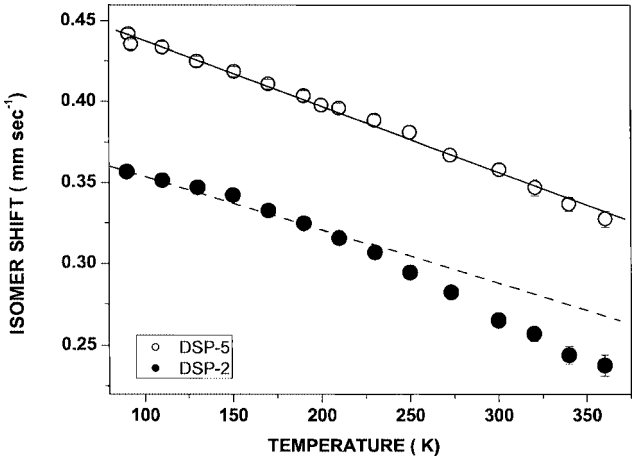

Figure 6. Temperature dependence of the isomer shift for [NMe_3Ph][**1**] ("DSP-2", filled circles) and **3b** ("DSP-5", open circles).

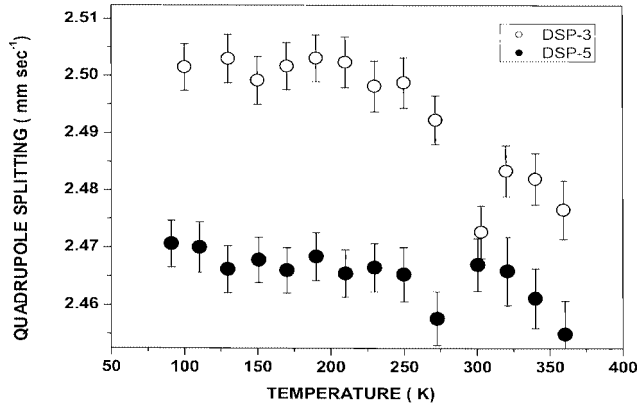

Figure 7. Temperature dependence of the quadrupole splitting for **3a** ("DSP-3") and **3b** ("DSP-5") showing the "normal" decrease with increasing temperature.

five-membered ring facing the metal atom. This larger value permits the resolution of the two components of the ME spectrum and the detailed temperature dependence of the QS parameter. The relevant data are summarized in Figure 8 which shows that in the low-temperature region (90 to ≈250 K) the QS parameter *increases* with increasing temperature, and then decreases normally in the higher temperature range. This relatively unusual behavior is not observed for the remainder of the Fe^{II} complexes as mentioned earlier.

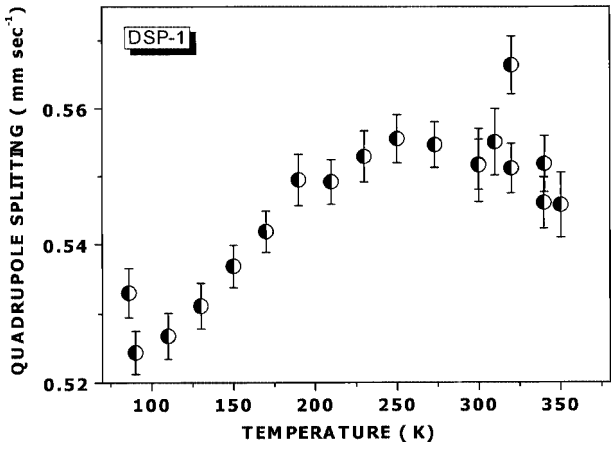

Figure 8. Temperature dependence of the quadrupole splitting for **1** ("DSP-1").

Recoil-Free Fraction and Vibrational Amplitude

For an optically "thin" absorber, the area under the resonance curve scales directly with the recoil-free fraction, f, of the 14.4 keV gamma ray of ^{57}Fe. Since $f = -\exp(k^2\langle x^2\rangle)$, where k is the wave vector of the gamma ray and $\langle x^2\rangle$ is the mean-square-amplitude-of-vibration (msav) of the metal atom, detailed information on the temperature dependence of the area under the resonance curve can provide information on the dynamics of the iron atom in a variety of environments. To this end, the temperature dependence of the logarithm under the resonance curve, $-\mathrm{d}\ln[A(T)/A(90)]/\mathrm{d}T$, has been determined for the ferracarboranes of the present study. A representative data set is summarized graphically in Figure 9 for [NMe_3Ph][**1**] and **3b**. Two qualitatively different types of behavior are reflected in the data listed in Table 1. In the case of **2c** and **3b**, the data are well-represented by a linear regression over the whole temperature range. More frequently, however, as in the case of the other compounds studied, the data are better represented by two different linear functions: one at low temperatures and one at high temperatures. In the case of **3d**, the data show continuous curvature over the accessible temperature range and have not been subjected to further analysis. As has been shown previously, using the slope of $\mathrm{d}\ln[A(T)/A(90)]/\mathrm{d}T$ it is possible to calculate $\langle x_{ave}{}^2\rangle$ from the ME data and compare this to the corresponding (average) value extracted from the $U_{i,j}$ data acquired in single-crystal X-ray diffraction studies. This comparison has been performed for three of the carboranes examined in this work, and these will now be discussed in some detail.

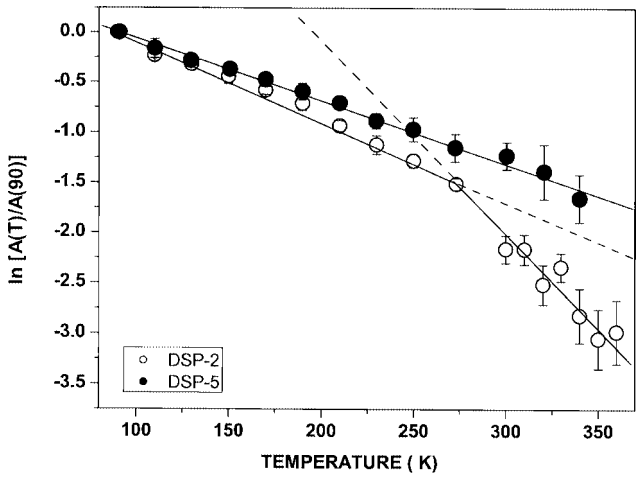

Figure 9. Temperature dependence of the logarithm of the area under the resonance curve for [NMe_3Ph][**1**] ("DSP-2") and **3b** ("DSP-5") showing the two types of dependencies discussed in the text.

For **1**, the ME f slope is $(8.00 \pm 0.09)\cdot 10^3\ K^{-1}$ with a correlation coefficient (R) of 0.992 for 11 data points. From this slope, $\langle x^2_{ave}\rangle = 0.021\ Å^2$ at 120 K, while the X-ray data yield a value of 0.0229 $Å^2$ at this temperature. In addition, the early X-ray data of Zalkin et al.[7] reflected a value of 0.053 $Å^2$ at room temperature, while the present ME data at 300 K yields $\langle x^2_{ave}\rangle = 0.045\ Å^2$ which is in reasonable agreement. A similar comparison for **3a** yields a value of $\langle x^2_{ave}\rangle = 0.0192\ Å^2$ at 120 K from the X-ray data of Kudinov et al.,[5] while the present ME data show $\langle x^2_{ave}\rangle = 0.0176\ Å^2$ at the same temperature. Finally, for **3b**, $\langle x^2_{ave}\rangle$ calculated from the X-ray data at 120 K is 0.0210 $Å^2$, while that extracted from the ME data is 0.0134 $Å^2$ which is only in modest agreement. Nonetheless, it is clear from this data, that the temperature dependence of f can provide a reasonable estimate of the msav of the metal atom in these compounds, and it can be used to compare the rmsav of the iron atom in different bonding environments.

The rmsav data for **3a** and **3b** at several different temperatures are summarized in Table 2, along with the corresponding data for ferrocene. This parameter is identical (within experimental error) for **3a** and ferrocene for all temperatures in the indicated range. In this context, the following correlation between the X-ray and ME data for **3a** and **3b** is significant. The corresponding rmsav data are displayed in Figure 10, which shows that this parameter is larger for **3a** than for **3b** over the whole temperature range, suggesting that the vibrational amplitude of the Fe atom in **3b** is smaller than it is for **3a**. This conclusion is in good agreement with the X-ray data at 120 K, which show that the average Fe–B bond lengths are 2.055 Å in **3b** and 2.085 Å in **3a**. Moreover, these results are also consistent with the DFT calculations which show that **3b** is 16.95 kcal mol^{-1} more stable than **3a**.[5]

Table 2. The rmsav [Å] for ferrocene, **3a**, and **3b**.

3b	**3a**	$FeCp_2$	*T* [K]
0.11	0.13	0.13	100
0.13	0.15	0.15	150
0.15	0.18	0.18	200
0.17	0.20	0.20	250
0.18	0.22	0.22	300

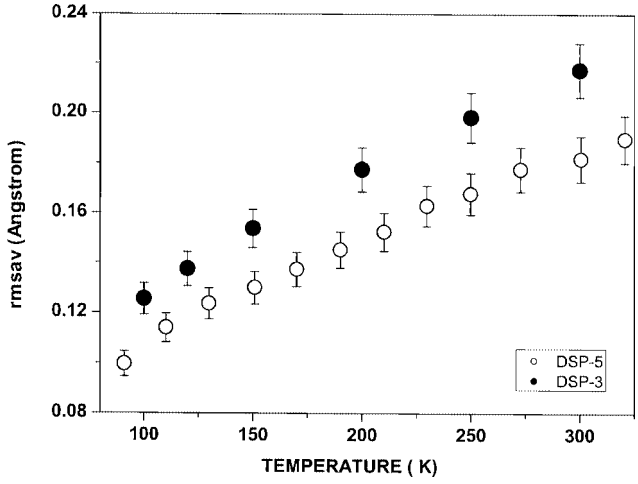

Figure 10. Temperature dependence of the rmsav of the iron atom in **3a** ("DSP-3") and **3b** ("DSP-5"). The larger vibrational amplitude is associated with the longer Fe–B bond lengths in the former than the latter compound as extracted from the 120 K X-ray data.

Electrochemistry

The redox activity of the Fe^{II} complexes shown in Scheme 1 was studied by electrochemical techniques. Before illustrating the redox aptitude of the ferratricarbollides, let us compare the classical (cyclopentadienyl)ferradicarbollide $[\mathbf{1}]^-$ with the charge-compensated analogs **2a**–**e** and bis(carboranyl) complex Fe(η-9-SMe_2-7,8-$C_2B_9H_{10})_2$ (**4**).

Since the Fe^{III} complex **1**, in MeCN solution, undergoes reversible reduction to the corresponding Fe^{II} monoanion,[20] it is not unexpected that $[\mathbf{1}]^-$, in CH_2Cl_2 solution, affords the complementary reversible Fe^{II}/Fe^{III} oxidation. In fact, exhaustive one-electron oxidation makes the original golden-yellow solution turn wine-red, and in confirmation of the chemical reversibility of the $[\mathbf{1}]^-/\mathbf{1}$ couple also in the long timescale of macroelectrolysis, cyclic voltammetric tests show a profile quite complementary to the original profile.

Similar behavior is displayed by complexes **2a**–**e**, except that the Fe^{II}/Fe^{III} oxidation occurs at markedly higher potential values, as illustrated in Table 3.

The charge compensation of the carborane ligand in 1-Cp-4-L-1,2,3,4-$Fe^{II}C_2B_9H_{10}$ makes the oxidation notably difficult with respect to the unsubstituted dicarbollyl ligand in $[\mathbf{1}]^-$, which is not only because of Coulombic effects, but in part also from the intrinsic electronic effect of the half-unit 9-L-7,8-$C_2B_9H_{10}$, as testified by the positive shift of the bis(carboranyl) derivative **4** relative to **2a**.[21] On the other hand, the methyl substitution at the carbon atoms of the carboranyl ligand in **2d** does not substantially have any effect with respect to **2a**, whereas the permethylation of the cyclopentadienyl ring in **2e** makes the oxidation significantly easier.

In order to evaluate the electronic effects played by the introduction of a third carbon atom in the framework of the classical dicarbollide dianion $[C_2B_9H_{11}]^{2-}$, Figure 11 compares the cyclic voltammetric behavior of complex **3c** with that of $[\mathbf{1}]^-$ in CH_2Cl_2 solution.

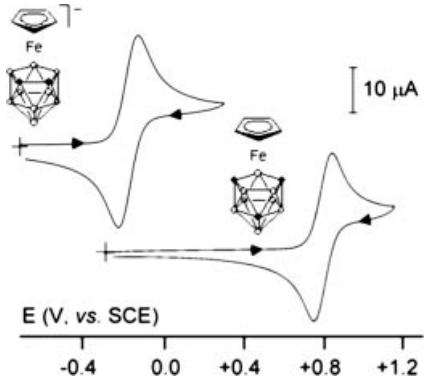

Figure 11. Cyclic voltammetric responses recorded at a platinum electrode in CH_2Cl_2 solutions of $[\mathbf{1}]^-$ ($1.3\cdot10^{-3}$ mol dm^{-3}) and **3c** ($1.2\cdot10^{-3}$ mol dm^{-3}); $[NBu_4][PF_6]$ (0.2 mol dm^{-3}) as supporting electrolyte; scan rate 0.2 V s^{-1}.

Similar to $[\mathbf{1}]^-$ and its charge-compensated derivatives, **3c** undergoes the reversible Fe^{II}/Fe^{III} step, but the oxidation is further shifted towards positive potential values. In fact, analysis of the cyclic voltammograms with scan rates varying from 0.02 to 2.00 V s^{-1} shows that (i) the current function $i_{pa}\cdot v^{-1/2}$ decreases by about 10% for each 10-fold in-

Table 3. Formal electrode potentials [V vs. SCE], peak-to-peak separations [mV], and color changes [λ_{max} in nm] accompanying the Fe^{II}/Fe^{III} oxidation of the dicarbollide complex $[\mathbf{1}]^-$ and the related charge-compensated complexes **2a**–**e** and **4** in CH_2Cl_2 solution.

Complex	$E°'$	ΔE_p[a]	Original color [λ_{max}]	Color of the oxidized solution [λ_{max}]
$[\mathbf{1}]^-$	–0.18	84	yellow	red-wine (570)
2a	+0.47	72	orange (475)	gray (594)
2b	+0.40	72	orange (470)	pink-brown (580)
2c	+0.40	62	red (415)	gray-green (593)
2d	+0.49	65	pink-orange (470)	green (615)
2e	+0.21	66	pale-orange (478)	olive-green (636; 710)
4[a]	+0.55	80	pink	pink-orange
$FeCp_2$	+0.39	80	yellow	green (618)

[a] Cf. with ref.[20]

crease of the scan rate, (ii) the current ratio i_{pc}/i_{pa} remains constantly equal to 1, and (iii) the peak-to-peak separation progressively increases from 84 to 154 mV. These parameters are diagnostic for a one-electron, chemically reversible, and electrochemically quasireversible process, in the short times of cyclic voltammetry.[22] Controlled-potential exhaustive oxidation (E_w = +1.0 V) consumes one electron *per* molecule. The original yellow solution turns pale green, and also in this case, the cyclic voltammetric test shows a profile quite complementary to the original profile.

Figure 12 compares the spectral changes accompanying the progressive passage from $[\mathbf{1}]^-$ to **1** (top) with those from **3c** to $[\mathbf{3c}]^+$ (bottom).

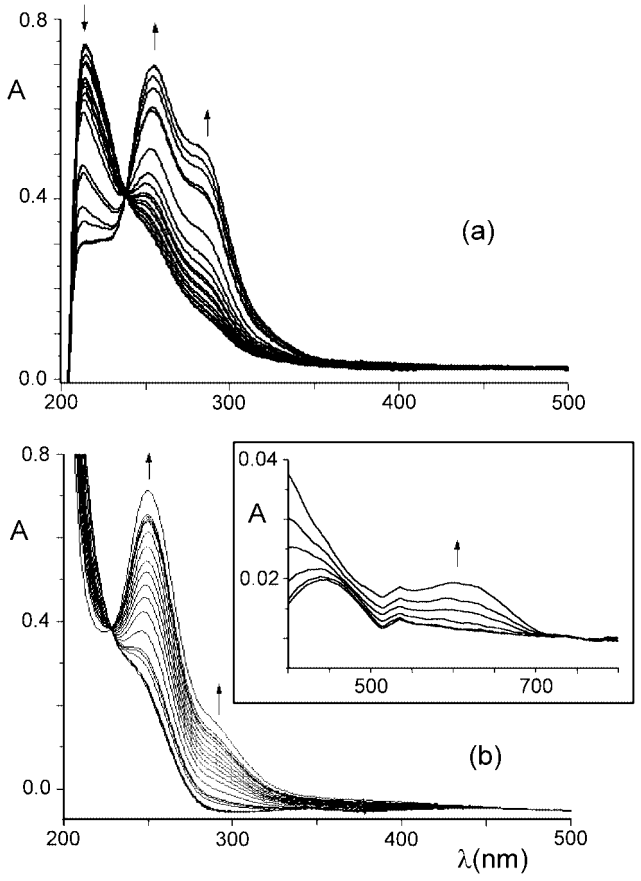

Figure 12. Spectral changes recorded in an OTTLE cell upon progressive oxidation of (a) $[\mathbf{1}]^-$ and (b) **3c**; CH_2Cl_2 solution with $[NBu_4][PF_6]$ (0.2 mol dm^{-3}) as supporting electrolyte.

In both cases, the appearance of the isosbestic point ($[\mathbf{1}]^-/\mathbf{1}$: λ = 238 nm; $\mathbf{3c}/[\mathbf{3c}]^+$: λ = 228 nm) further supports the chemical reversibility of the pertinent oxidation processes. The bands arising in the UV region are conceivably assigned to LMCT transitions. In agreement with the final pale-green color of the solution of $[\mathbf{3c}]^+$, a weak band also appears at λ_{max} = 620 nm (inset of Figure 12).

A similar redox activity holds in THF solution, except that, because of the larger cathodic window of this solvent, a reduction process can also be detected, which possesses features of chemical reversibility in the cyclic voltammetric timescale (see Figure 13).

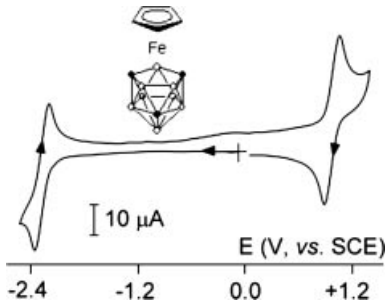

Figure 13. Cyclic voltammetric response recorded at a gold electrode in THF solution of **3c** ($1.0\cdot10^{-3}$ mol dm^{-3}); $[NBu_4][PF_6]$ (0.2 mol dm^{-3}) as supporting electrolyte; scan rate 0.2 V s^{-1}.

The extremely negative potential value of the process prevented the experimental measurement by controlled-potential coulometry of the number of electrons involved, but the similarity of the peak height with that of the anodic process suggests it is a one-electron process. In the first instance, we therefore assign it to the Fe^{II}/Fe^{I} passage; a redox change not too unusual in organometallic chemistry,[23] but quite new in ferracarborane chemistry. The separation between the one-electron oxidation and the one-electron reduction (3.2 eV) can be roughly considered as an experimental measurement of the HOMO–LUMO separation.

Complexes **3b** and **3d** also display a chemically reversible one-electron oxidation. However, in contrast to **3c**, no reduction process is detected in THF for complex **3d**, whereas complex **3b** gives rise to an irreversible reduction. Upon exhaustive oxidation, the original orange solution of complex **3b** turns brown, and the spectroelectrochemical trend in the UV region is very similar to that illustrated for **3c**. A similar spectroelectrochemical pattern was recorded in the UV region during the golden-yellow/maroon transition from **3d** to $[\mathbf{3d}]^+$, except for a new band at 350 nm (see Supporting Information).

Finally, the one-electron oxidation of complex **3a** in CH_2Cl_2 solution is accompanied by chemical complica-

Table 4. Formal electrode potentials [V vs. SCE], peak-to-peak separations [mV], and current ratios for the redox activity of the ferratricarbollides **3a**–**d**.

	Oxidation			Reduction			Solvent
	$E°'$	ΔE_p[a]	i_{pc}/i_{pa}[a]	$E°'$	ΔE_p[a]	i_{pa}/i_{pc}[a]	
$[\mathbf{1}]^-$	–0.18	84	1.0	–	–	–	CH_2Cl_2
	–0.04	89	1.0	–	–	–	THF
3a	+0.74	72	0.8[b]	–	–	–	CH_2Cl_2
	+0.91	103	0.5	–1.56	74	0.5	THF
3b	+0.82	73	1.0	–	–	–	CH_2Cl_2
	+0.94	72		–2.05[c]	–	1.0	THF
3c	+0.80	82	1.0	–	–	–	CH_2Cl_2
	+0.96	96	1.0	–2.29	127	0.8[d]	THF
3d	+0.60	73	1.0	–	–	–	CH_2Cl_2
	+0.77	78	1.0	–	–	–	THF
$FeCp_2$	+0.39	80	1.0	–	–	–	CH_2Cl_2
	+0.53	82	1.0	–	–	–	THF

[a] Measured at 0.1 V s^{-1}. [b] Accompanied by chemical complications (see text). [c] Peak-potential value for irreversible processes. [d] Because of the close solvent discharge, the present value is of limited accuracy as far as the extent of chemical reversibility is concerned.

tions. The current ratio i_{pc}/i_{pa} is lower than unity at low scan rate and progressively tends to increase with an increase of the scan rate. In fact, exhaustive one-electron oxidation leads to a presently unknown species, which reduces at $E°' = +0.34$ V. The Fe^{II}/Fe^{I} reduction in THF (in such solvent the complex is stable only for short times) is also partially chemically reversible and occurs at potential values less negative than that of **3c**. In fact, a HOMO–LUMO separation of 2.5 eV can be calculated. The formal electrode potentials of the mentioned electrode processes are compiled in Table 4.

Conclusions

The X-ray diffraction study revealed that the Fe···C_2B_3 and Fe···Cp distances in 17-electron ferracarborane **1** are significantly longer than those in its 18-electron congener $[\mathbf{1}]^-$, in accordance with one-electron removal from the bonding HOMO. The electrochemical investigation revealed that the Fe^{II}-tricarbollide complexes are more difficult to oxidize than the charge-compensated dicarbollide analogs, which in turn are more difficult to oxidize than the parent ferracarborane $[\mathbf{1}]^-$. The location of the Fe^{II}/Fe^{III} couple for **3a**–**c** at highly positive potential values makes the Fe^{II}/Fe^{I} reduction accessible. The fact that the redox changes of the different isomers occur at different potential values constitutes a further supporting technique in their selective recognition. Temperature-dependent ^{57}Fe Mössbauer effect spectroscopy (TDMES) was used to elucidate the hyperfine interaction parameters of the neutral carbollide complexes, as well as the dynamical aspects of the iron atom motion as a function of temperature. For a number of ferracarboranes studied in detail, modestly good agreement, within experimental error, was obtained for the msav extracted from single-crystal X-ray diffraction studies and TDMES.

Experimental Section

General Remarks: All reactions were carried out under argon in anhydrous solvents which were purified and dried using standard procedures. The isolation of products was conducted in air. Ferracarboranes **1**, $[NMe_3Ph][\mathbf{1}]$,[20] and **3a**–**d**[5,6] were prepared as described in the literature. The solutions of sodium salts Na[9-L-7,8-R_2-7,8-$C_2B_9H_8$] were obtained by reaction of the corresponding carborane with NaH in THF.[24] Irradiation was conducted in a Schlenk tube using a high-pressure mercury-vapor lamp with a phosphor-coated bulb (400 W). The ^1H- and ^{11}B NMR spectra were measured with a Bruker AMX-400 instrument at room temp. in [D_6]acetone unless otherwise stated. Materials and apparatus for electrochemistry and spectroelectrochemistry have been described elsewhere.[25] All the potential values are referred to the saturated calomel electrode (SCE).

1-Cp-4-SMe_2-1,2,3-$FeC_2B_9H_{10}$ (2a): To a solution of [$CpFe(C_6H_6)$]-PF_6 (344 mg, 1 mmol) in a mixture of THF (16 mL) and MeCN (4 mL) which was chilled to –78 °C, was added a solution of Na[9-SMe_2-7,8-$C_2B_9H_{10}$] in THF (4 mL, 1 mmol). The resulting mixture was irradiated with stirring at –60 to –40 °C within 1 h, and the solvents evaporated in vacuo. The residue was washed several times with MeOH giving red solid **2a** which was 95% pure according to ^1H- and ^{11}B NMR spectroscopy. The analytically pure sample was obtained by reprecipitation using heptane from CH_2Cl_2. Yield 255 mg (80%). ^1H NMR: $\delta = 4.54$ (s, 5 H, Cp), 4.08 (br. s, 1 H, cage CH), 3.52 (br. s, 1 H, cage CH), 2.73 (s, 3 H, SMe_2), 2.73 (s, 3 H, SMe_2) ppm. ^{11}B NMR (*J*, Hz): $\delta = -6.04$ (d, 136, 1B), –6.04 (s, 1B, $BSMe_2$), –10.20 (d, 142, 1B), –11.30 (d, 142, 1B), –13.24 (d, 142, 1B), –17.87 (d, 138, 1B), –24.55 (d, 152, 1B), –27.11 (d, 165, 1B), –28.71 (d, 202, 1B) ppm. $C_9H_{21}B_9FeS$ (314.46): calcd. C 34.38, H 6.73, B 30.94, Fe 17.76; found C 34.32, H 6.48, B 30.80, Fe 17.44.

1-Cp-4-NMe_3-1,2,3-$FeC_2B_9H_{10}$ (2b): Compound **2b** was synthesized in a similar manner to **2a**. However, when the irradiation was finished, the reaction tube was placed into a Dewar vessel with an acetone/dry ice mixture, and the reaction mixture was additionally stirred for 24 h with gradual rising of temp. to 20 °C. Yield 32%. ^1H NMR: $\delta = 4.63$ (s, 5 H, Cp), 4.56 (br. s, 1 H, cage CH), 3.58 (br. s, 1 H, cage CH), 3.19 (s, 9 H, NMe_3) ppm. ^{11}B NMR (*J*, Hz): $\delta = 5.27$ (s, 1B, $BNMe_3$), –5.45 (d, 129, 1B), –10.13 (d, 130, 1B), –10.84 (d, 109, 1B), –13.31 (d, 156, 1B), –14.94 (d, 151, 1B), –24.85 (d, 152, 1B), –26.08 (d, 157, 1B), –28.30 (d, 167, 1B) ppm. $C_{10}H_{24}B_9FeN$ (311.44): calcd. C 38.57, H 7.77, N 4.50; found C 38.59, H 7.91, N 4.54.

1-Cp-4-py-1,2,3-$FeC_2B_9H_{10}$ (2c): To a solution of [$CpFe(C_6H_6)$]PF_6 (172 mg, 0.5 mmol) in a mixture of THF (3 mL) and MeCN (3 mL) which was chilled to –78 °C, was added a solution of Na[9-py-7,8-$C_2B_9H_{10}$] in THF (10 mL, 0.5 mmol). The resulting mixture was irradiated with stirring at –60 to –40 °C within 3 h, treated with MeOH (1 mL), and filtered. The filtrate was evaporated in vacuo, and the residue was eluted on a silica gel column (7 cm) with a CH_2Cl_2/petroleum ether (1:1) mixture. The bright-red band was collected, evaporated in vacuo, and washed several times with ether to give dark-red crystals of **2c**. Yield 60 mg (48%). ^1H NMR: $\delta =$ 9.00 (d, 5.6, 2 H, C_5H_5N), 8.46 (t, 7.6, 1 H, C_5H_5N), 8.00 (t, 7.2, 2 H, C_5H_5N), 4.72 (br. s, 1 H, cage CH), 4.15 (s, 5 H, Cp), 3.53 (br. s, 1 H, cage CH) ppm. ^{11}B NMR (*J*, Hz): $\delta = 2.56$ (s, 1B, Bpy), –5.68 (d, 129, 1B), –9.83 (d, 147, 1B), –11.03 (d, 158, 1B), –12.64 (d, 141, 1B), –13.72 (d, 139, 1B), –23.03 (d, 153, 1B), –25.92 (d, 151, 1B), –28.05 (d, 167, 1B) ppm. $C_{12}H_{20}B_9FeN$ (331.43): calcd. C 43.49, H 6.08, B 29.35; found C 43.49, H 6.02, B 29.08.

1-Cp-2,3-Me_2-4-SMe_2-1,2,3-$FeC_2B_9H_8$ (2d): Compound **2d** was prepared in a similar manner to **2a**. Yield 220 mg (64%). ^1H NMR: $\delta = 4.48$ (s, 5 H, Cp), 2.86 (s, 3 H, SMe_2), 2.60 (s, 3 H, SMe_2), 2.44 (s, 3 H, CMe), 2.22 (s, 3 H, CMe) ppm. ^{11}B NMR (*J*, Hz; CD_2Cl_2): $\delta = -1.65$ (s, 1B, BPy), –4.86 (d, 157, 1B), –6.20 (d, 155, 1B), –9.35 (d, 142, 1B), –12.66 (d, 138, 1B), –17.68 (d, 130, 2B), –18.55 (d, 140, 1B), –20.64 (d, 150, 1B) ppm. $C_{11}H_{26}B_9FeS$ (343.52): calcd. C 38.46, H 7.63; found C 38.39, H 7.21.

1-Cp*-4-SMe_2-1,2,3-$FeC_2B_9H_{10}$ (2e): A solution of Na[9-SMe_2-7,8-$C_2B_9H_{10}$] in THF (2 mL, 0.5 mmol) was added to a solution of [$Cp^*Fe(MeCN)_3$]BF_4 (200 mg, 0.5 mmol) in THF (10 mL) at 0 °C. The resulting mixture was stirred at this temp. for 1 h, and compound **2e** was isolated in a similar manner to **2a**. Yield 155 mg (80%). ^1H NMR: $\delta = 5.32$ (br. s, 1 H, cage CH), 3.58 (br. s, 1 H, cage CH), 2.59 (s, 6 H, SMe_2), 2.39 (s, 6 H, SMe_2), 2.35 (br. s, 1 H, cage CH), 1.79 (s, 15 H, Cp*) ppm. ^{11}B NMR (*J*, Hz): $\delta =$ –4.90 (d, 195, 1B), –6.02 (s, 1B, $BSMe_2$), –9.19 (d, 144, 1B), –12.90 (d, 130, 1B), –13.80 (d, 130, 1B), –18.18 (d, 138, 1B), –25.28 (d, 159, 1B), –27.27 (d, 176, 1B), –29.13 (d, 227, 1B) ppm.

Mössbauer Spectroscopy: The solid compounds were transferred to plastic sample holders and examined by standard transmission

Table 5. Crystal data and structure-refinement parameters for **1**, [NMe_3Ph][**1**], and **2b**.

Compound	**1**	[NMe_3Ph][**1**]	**2b**
Empirical formula	$C_7H_{16}B_9Fe$	$C_{16}H_{30}B_9FeN$	$C_{10}H_{23}B_9FeN$
Formula weight	253.34	389.55	310.43
Crystal color, habit	violet plate	red plate	red prism
Crystal size [mm]	0.30×0.10×0.10	0.40×0.10×0.10	0.30×0.20×0.20
Temperature [K]	120(2)	120(2)	120(2)
Crystal system	monoclinic	monoclinic	orthorhombic
Space group	$P2_1/c$	$P2_1/n$	$Pna2_1$
a [Å]	11.4669(1)	8.2460(2)	14.846(2)
b [Å]	6.4619(1)	16.9626(5)	8.788(1)
c [Å]	16.6791(2)	14.3504(4)	11.827(2)
β [°]	100.650(1)	96.8406(16)	90
V [Å^3]	1214.60(3)	1992.95(9)	1543.1(4)
$Z(Z')$	4(1)	4(1)	4(1)
$F(000)$	516	816	644
$D_{calcd.}$ [g cm^{-1}]	1.385	1.298	1.336
Linear absorption, μ [cm^{-1}]	11.99	7.57	9.59
T_{min}/T_{max}	0.7150/0.8895	0.7516/0.9281	0.7619/0.8314
Scan type	ω	ω	ω
θ range [°]	1.81–45.00	1.87–50.34	2.69–30.01
Completeness of dataset [%]	98.4	98.1	99.9
Reflections measured	36197	71800	11745
Independent reflections	9862 [R_{int} = 0.0456]	20808 [0.0396]	4327 [0.0276]
Observed reflections [$I > 2\sigma(I)$]	7912	15599	3148
Parameters	218	364	247
Final $R(F_{hkl})$:R_1 ratio	0.0435	0.0431	0.0475
wR_2	0.0981	0.0894	0.1169
GOF	1.014	0.993	0.945
$\Delta\rho_{max}$, $\Delta\rho_{min}$ [e Å^{-3}]	0.628, –0.636	0.669, –0.544	0.969, –0.760

Mössbauer effect spectroscopy (MES) using a 50 mCi ^{57}Co/Rh source as described previously.[26] Spectrometer calibration was performed using a 10 mg cm^{-2} α-Fe foil at room temp., and all isomer shifts are referred to the centroid of such a spectrum. ME data acquisition times varied from 7 to 30 h (depending on the temp.), and since one of the objectives of this research was to elucidate the temperature-dependent parameters extracted from the ME data, the thermal variation with time was continuously monitored using the Daswin program of Glaberson and Brettschneider.[27] The temp. uncertainties are estimated as ±0.1 K over the data acquisition intervals.

Calculation Details: All calculations were performed using Gaussian 98 package.[28] The structure of [**1**]$^-$ was optimized at B3LYP/6-31G* level in C_s symmetry. The molecular orbital visualization was performed by ChemCraft software, version 1.5 (www.chemcraftprog.org).

X-ray Crystallography: Crystals of **1** and [NMe_3Ph][**1**] suitable for X-ray diffraction were grown by slow evaporation of CH_2Cl_2 solutions. Crystals of **2b** were grown by slow diffusion in a two-layer system, solution of the complex in [D_6]acetone/petroleum ether, placed in an NMR tube. X-ray diffraction experiments were carried out with a Bruker SMART 1000 CCD area detector, using graphite-monochromated Mo-K_α radiation at 110 K. Low temp. of the crystals was maintained with a Cryostream (Oxford Cryosystems) open-flow nitrogen gas cryostat. Reflection intensities were integrated using SAINT software,[29] and absorption correction was applied semi-empirically using SADABS program. The structures were solved by direct method and refined by the full-matrix least-squares against F^2 in anisotropic approximation for non-hydrogen atoms. All polyhedron hydrogen atoms were located from the Fourier density synthesis and refined in isotropic approximation. Crystal data and structure-refinement parameters for **1**, [NMe_3Ph][**1**], and **2b** are given in Table 5. All calculations were performed using the SHELXTL software.[30]

CCDC-291166 (for [NMe_3Ph][**1**]), -291167 (for **1**), and -291168 (for **2b**) contain the supplementary crystallographic data for this paper. These data can be obtained free of charge from The Cambridge Crystallographic Data Centre via www.ccdc.cam.ac.uk/data_request/cif.

Supporting Information (for details see the footnote on the first page of this article): Spectroelectrochemical data for transition from **3d** to [**3d**]$^+$ and the optimized coordinates from DFT calculations of [**1**]$^-$.

Acknowledgments

We thank Prof. W. Glaberson and Dr. M. Brettschneider for the use of their Daswin program prior to publication. Financial support from the Racah Institute and the Division of General Chemistry and Material Sciences of Russian Academy of Sciences, as well as the University of Siena (PAR 2005) is also gratefully acknowledged. D. S. P. thanks INTAS for a Young Scientist Fellowship (Grant No. 04-83-3848).

[1] M. F. Hawthorne, R. L. Pilling, *J. Am. Chem. Soc.* **1965**, *87*, 3987–3988.
[2] Synthesis of **2a** and **2e** was described in a short communication: A. R. Kudinov, V. I. Meshcheryakov, P. V. Petrovskii, M. I. Rybinskaya, *Izv. Akad. Nauk, Ser. Khim.* **1999**, 177–179; *Russ. Chem. Bull.* **1999**, *48*, 176–177 *(Engl. Transl.)*.
[3] T. P. Gill, K. R. Mann, *Inorg. Chem.* **1983**, *22*, 1986–1991.
[4] Complex **2e** was prepared earlier in 30% yield by reaction of the corresponding anion with [Cp*FeCl]$_2$: Y.-K. Yan, D. M. P. Mingos, T. E. Müller, D. J. Williams, M. Kurmoo, *J. Chem. Soc., Dalton Trans.* **1995**, 2509–2514.

[5] D. S. Perekalin, J. Holub, D. G. Golovanov, K. A. Lyssenko, P. V. Petrovskii, B. Štibr, A. R. Kudinov, *Organometallics* **2005**, *24*, 4387–4392.
[6] J. Holub, B. Grüner, D. S. Perekalin, D. G. Golovanov, K. A. Lyssenko, P. V. Petrovskii, A. R. Kudinov, B. Štibr, *Inorg. Chem.* **2005**, *44*, 1655–1659.
[7] A. Zalkin, D. H. Templeton, T. E. Hopkins, *J. Am. Chem. Soc.* **1965**, *87*, 3988–3990.
[8] The numbering system where the metal vertex bears number 1 is used for metallacarboranes.
[9] A. Haaland, J. E. Nilsson, *Acta Chem. Scand.* **1968**, *23*, 2653–2670.
[10] B. M. Yamin, H. K. Fun, K. Sivakumar, B. C. Yip, O. B. Shawkataly, *Acta Crystallogr. Sect. C* **1996**, *52*, 600–602, and references therein.
[11] The ^{2}E ground state of **1** is in accordance with low-temperature EPR data: A. H. Maki, T. E. Berry, *J. Am. Chem. Soc.* **1965**, *87*, 4437–4441.
[12] a) V. I. Goldansakii, E. F. Makarov in *Chemical Applications of Mössbauer Spectroscopy* (Eds.: V. I. Goldanskii, R. H. Herber), Academic Press, New York, **1968**, pp. 47–55; b) B. D. Dunlap, G. M. Kalvius in *Mössbauer Isomer Shifts* (Eds.: G. K. Shenoy, F. E. Wagner), North Holland Publishing, Amsterdam, **1978**, pp. 15–48.
[13] R. H. Herber in *Chemical Mössbauer Spectroscopy* (Ed.: R. H. Herber), Plenum Press, New York, **1984**, pp. 199–216.
[14] I. Nowik, R. H. Herber, *Inorg. Chim. Acta* **2000**, *310*, 191–195; I. Nowik, R. H. Herber, *Hyperfine Interact.* **2005**, in press.
[15] R. L. Collins, *J. Chem. Phys.* **1965**, *42*, 1072–1080.
[16] See the discussion in: N. N. Greenwood, T. C. Gibb, *Mössbauer Spectroscopy*, Chapman and Hall, London, **1971**, pp. 233–236.
[17] H. Schottenberger, K. Wurst, U. J. Griesser, R. K. R. Jetti, G. Laus, R. H. Herber, I. Nowik, *J. Am. Chem. Soc.* **2005**, *127*, 6795–6801.
[18] R. H. Herber, I. Gattinger, F. H. Köhler, *Inorg. Chem.* **2000**, *39*, 851–853.
[19] H. Schottenberger, K. Wurst, R. H. Herber, *J. Organomet. Chem.* **2001**, *625*, 200–207.
[20] M. F. Hawthorne, D. C. Young, T. D. Andrews, D. V. Howe, R. L. Pilling, A. D. Pitts, M. Reintjes, L. F. Warren Jr., P. A. Wegner, *J. Am. Chem. Soc.* **1968**, *90*, 879–896.
[21] Y.-K. Yan, D. M. P. Mingos, T. E. Müller, D. J. Williams, M. Kurmoo, *J. Chem. Soc., Dalton Trans.* **1994**, 1735–1741.
[22] P. Zanello, *Inorganic Electrochemistry: Theory, Practice, and Application*, RSC, United Kingdom, **2003**.
[23] a) M. C. Rakowski, D. H. Bush, *J. Am. Chem. Soc.* **1975**, *97*, 2570–2571; b) A. Croisy, D. Lexa, M. Momenteau, J. M. Saveant, *Organometallics* **1985**, *4*, 1574–1579; c) M. H. Desbois, D. Astruc, J. Guillin, J. P. Mariot, F. Varret, *J. Am. Chem. Soc.* **1985**, *107*, 5280–5282; d) K. R. Rodgers, R. A. Reed, Y. O. Su, T. G. Spiro, *Inorg. Chem.* **1992**, *31*, 2688–2700; e) C. Bianchini, F. Laschi, D. Masi, F. M. Ottaviani, A. Pastor, M. Peruzzini, P. Zanello, F. Zanobini, *J. Am. Chem. Soc.* **1993**, *115*, 2723–2730; f) D. Mimica, J. H. Zagal, F. Bedioui, *J. Electroanal. Chem.* **2001**, *497*, 106–143; g) S. Rigaut, M.-H. Delville, J. Losada, D. Astruc, *Inorg. Chim. Acta* **2002**, *334*, 225–242.
[24] V. I. Meshcheryakov, P. S. Kitaev, K. A. Lyssenko, Z. A. Starikova, P. V. Petrovskii, Z. Janoušek, M. Corsini, F. Laschi, P. Zanello, A. R. Kudinov, *J. Organomet. Chem.* **2005**, *690*, 4745–4754.
[25] F. Fabrizi de Biani, M. Corsini, P. Zanello, H. Yao, M. E. Bluhm, R. N. Grimes, *J. Am. Chem. Soc.* **2004**, *126*, 11360–11369.
[26] R. H. Herber, I. Nowik, D. A. Loginov, Z. A. Starikova, A. R. Kudinov, *Eur. J. Inorg. Chem.* **2004**, 3476–3483, and references therein.
[27] W. Glaberson, M. Brettschneider; see: www.PHYS.HUJI.AC.IL/~glabersn.
[28] M. J. Frisch, G. W. Trucks, H. B. Schlegel, G. E. Scuseria, M. A. Robb, J. R. Cheeseman, V. G. Zakrzewski, J. A. Montgomery Jr., R. E. Stratmann, J. C. Burant, S. Dapprich, J. M. Millam, A. D. Daniels, K. N. Kudin, M. C. Strain, O. Farkas, J. Tomasi, V. Barone, M. Cossi, R. Cammi, B. Mennucci, C. Pomelli, C. Adamo, S. Clifford, J. Ochterski, G. A. Petersson, P. Y. Ayala, Q. Cui, K. Morokuma, D. K. Malick, A. D. Rabuck, K. Raghavachari, J. B. Foresman, J. Cioslowski, J. V. Ortiz, B. B. Stefanov, G. Liu, A. Liashenko, P. Piskorz, I. Komaromi, R. Gomperts, R. L. Martin, D. J. Fox, T. Keith, M. A. Al-Laham, C. Y. Peng, A. Nanayakkara, C. Gonzalez, M. Challacombe, P. M. W. Gill, B. G. Johnson, W. Chen, M. W. Wong, J. L. Andres, M. Head-Gordon, E. S. Replogle, J. A. Pople, *Gaussian 98*, revision A.7, Gaussian, Inc., Pittsburgh, PA, **1998**.
[29] SMART V5.051 and SAINT V5.00, Area detector control and integration software, Bruker AXS Inc., Madison,WI-53719, USA, **1998**.
[30] G. M. Sheldrick, SHELXTL-97, V5.10, Bruker AXS Inc., Madison, WI-53719, USA, **1997**.

Received: December 22, 2005
Published Online: March 22, 2006

